

Origin of low thermal conductivity in In₄Se₃

Article

Accepted Version

Luu, S. D. N., Supka, A. R., Nguyen, V. H., Vo, D.-V., Hung, N., Wojciechowski, K. T., Fornari, M. and Vaqueiro, P. ORCID: <https://orcid.org/0000-0001-7545-6262> (2020) Origin of low thermal conductivity in In₄Se₃. ACS Applied Energy Materials, 3 (12). pp. 12549-12556. ISSN 2574-0962 doi: <https://doi.org/10.1021/acsaem.0c02489> Available at <https://centaur.reading.ac.uk/94436/>

It is advisable to refer to the publisher's version if you intend to cite from the work. See [Guidance on citing](#).

To link to this article DOI: <http://dx.doi.org/10.1021/acsaem.0c02489>

Publisher: ACS Publications

All outputs in CentAUR are protected by Intellectual Property Rights law, including copyright law. Copyright and IPR is retained by the creators or other copyright holders. Terms and conditions for use of this material are defined in the [End User Agreement](#).

www.reading.ac.uk/centaur

CentAUR

Central Archive at the University of Reading

Reading's research outputs online

This document is confidential and is proprietary to the American Chemical Society and its authors. Do not copy or disclose without written permission. If you have received this item in error, notify the sender and delete all copies.

Origin of Low Thermal Conductivity in In₄Se₃

Journal:	<i>ACS Applied Energy Materials</i>
Manuscript ID	ae-2020-02489q.R1
Manuscript Type:	Article
Date Submitted by the Author:	13-Nov-2020
Complete List of Authors:	Luu, Son D N; Institute of Research and Development, Duy Tan Univeristy Supka, Andrew ; Department of Physics and Science of Advanced Materials Program Nguyen, Van Huy ; Key Laboratory of Advanced Materials for Energy and Environmental Applications Vo, Dai-Viet N. ; Center of Excellence for Green Energy and Environmental Nanomaterials (CE@GrEEN) Tuan Hung, Nguyen; Tohoku University , Frontier Research Institute for Interdisciplinary Sciences Wojciechowski, Krzysztof; AGH University of Science and Technology, faculty of Materials Science and Ceramics Fornari, Marco; Central Michigan University, Physics Vaqueiro, Paz; University of Reading, Chemistry

SCHOLARONE™
Manuscripts

Origin of Low Thermal Conductivity in In_4Se_3

Son D. N. Luu^{1*}, *Andrew R. Supka*², *Van Huy Nguyen*³, *Dai-Viet N. Vo*⁴, *Nguyen T. Hung*⁵,
Krzysztof T. Wojciechowski^{6,7}, *Marco Fornari*², *Paz Vaqueiro*^{8*}

¹Institute of Research and Development, Duy Tan University, Da Nang, 550000, Viet Nam

²Department of Physics and Science of Advanced Materials Program, Central Michigan University, Mt. Pleasant, Michigan, 48859 USA

³Key Laboratory of Advanced Materials for Energy and Environmental Applications, Lac Hong University, Dong Nai 810000, Viet Nam

⁴Center of Excellence for Green Energy and Environmental Nanomaterials (CE@GrEEN), Nguyen Tat Thanh University, 300A Nguyen Tat Thanh, District 4, Ho Chi Minh City 755414, Viet Nam

⁵Frontier Research Institute for Interdisciplinary Sciences, Tohoku University, Sendai, 980-8578, Japan

⁶ AGH University of Science and Technology, Faculty of Materials Science and Ceramics, Thermoelectric Research Laboratory, 30 Mickiewicza, 30-059 Cracow, Poland

⁷ The Lukasiewicz Research Network –, The Institute of Advanced Manufacturing Technology, Centre of Thermoelectric Materials Research, 37A Wroclawska, 30-011 Cracow, Poland

⁸Department of Chemistry, University of Reading, Whiteknights Park, Reading RG6 6AD, England, United Kingdom

Abstract

In₄Se₃ is an attractive *n*-type thermoelectric material for mid-range waste heat recovery, owing to its low thermal conductivity ($\sim 0.9 \text{ W}\cdot\text{m}^{-1}\cdot\text{K}^{-1}$ at 300 K). Here, we explore the relationship between the elastic properties, thermal conductivity and structure of In₄Se₃. The experimentally-determined average sound velocity (2010 m s⁻¹), Young's modulus (47 GPa), and Debye temperature (198 K) of In₄Se₃ are rather low, indicating considerable lattice softening. This behavior, which is consistent with low thermal conductivity, can be related to the complex bonding found in this material, in which strong covalent In-In and In-Se bonds coexist with weaker electrostatic interactions. Phonon dispersion calculations show that Einstein-like modes occur at $\approx 30 \text{ cm}^{-1}$. These Einstein-like modes can be ascribed to weakly bonded In⁺ cations located between strongly-bonded [(In₃)⁵⁺(Se²⁻)₃]⁻ layers. The Grüneisen parameter for the soft-bonded In⁺ at the frequencies of the Einstein-like modes is large, indicating a high degree of bond anharmonicity and hence increased phonon scattering. The calculated thermal conductivity and elastic properties are in good agreement with experimental results.

1
2
3
4
5
6
7
8
9
10
11
12
13
14
15
16
17
18
19
20
21
22
23
24
25
26
27
28
29
30
31
32
33
34
35
36
37
38
39
40
41
42
43
44
45
46
47
48
49
50
51
52
53
54
55
56
57
58
59
60

Keywords

Thermoelectric materials, Thermal conductivity, Grüneisen parameter, Lattice softening, Lone pair.

INTRODUCTION

Worldwide concerns with energy supply and sustainability have stimulated considerable research efforts into thermoelectric materials, which enable direct conversion of waste heat into electrical power. The efficiency of thermoelectric energy recovery is related to the dimensionless thermoelectric figure of merit, ZT , which is given by $ZT = S^2 \sigma T / (\kappa_L + \kappa_e)$ where S , σ , T , κ_L , and κ_e are the Seebeck coefficient, electrical conductivity, absolute temperature, lattice, and electronic thermal conductivities, respectively¹. To maximize ZT , materials with low thermal conductivity are required. As a consequence of Wiedemann-Franz law, reducing the electronic thermal conductivity, κ_e , would simultaneously lower the electrical conductivity, σ . Therefore, strategies to reduce the thermal conductivity focus on the lattice component (κ_L), which is related to vibrational energy transport. These strategies include the introduction of species with low-energy localized vibrational modes (the phonon-glass electron-crystal (PGEC) approach)^{2,3,4} designing materials with part-crystalline part-liquid states (the phonon-liquid electron-crystal (PLEC) approach)^{4,5,6,7,8}, grain-boundary engineering^{9, 10}, and the introduction of nano-inclusions^{10,11}.

1
2
3
4 Understanding the origin of the intrinsically low lattice thermal conductivity found in some
5
6
7 thermoelectric materials is critically important to facilitate the discovery of the next generation of
8
9
10 high-performance candidates^{12,16}. Pseudo-layered In_4Se_3 (Figure 1), a mixed-valence
11
12
13 compound that can be formulated as $(\text{In}^+)[(\text{In}_3)^{5+}(\text{Se}^{2-})_3]^-$, is one of the best performing *n*-type
14
15
16 thermoelectric materials for mid-range waste heat recovery^{17,32}. The thermoelectric properties
17
18
19 of In_4Se_3 are highly anisotropic due to its pseudo-layered structure. Single crystals of $\text{In}_4\text{Se}_{3-\delta}$ (δ
20
21
22 = 0.65) exhibit an impressive $ZT \approx 1.48$ at 705 K in the direction parallel to the layers, but a much
23
24
25 lower ZT , < 0.5 , perpendicular to the layers¹⁷. It has been reported that multiple doping is an
26
27
28 effective strategy to produce polycrystalline samples with similarly high values of ZT , as
29
30
31 exemplified by Pb/Sn-co-doped In_4Se_3 ¹⁹ ($ZT = 1.4$ at 733 K). The outstanding thermoelectric
32
33
34 performance of In_4Se_3 has been attributed to its low thermal conductivity, which is $\sim 0.9 \text{ W}\cdot\text{m}^{-1}\cdot\text{K}^{-1}$
35
36
37 for the undoped polycrystalline material at room temperature^{17,18,19,32}, while in doped and
38
39
40 selenium-deficient samples, values as low as $\sim 0.4 \text{ W}\cdot\text{m}^{-1}\cdot\text{K}^{-1}$ at 723 K can be reached^{30,31}.
41
42
43
44
45
46
47
48
49
50
51
52
53
54
55
56
57
58
59
60

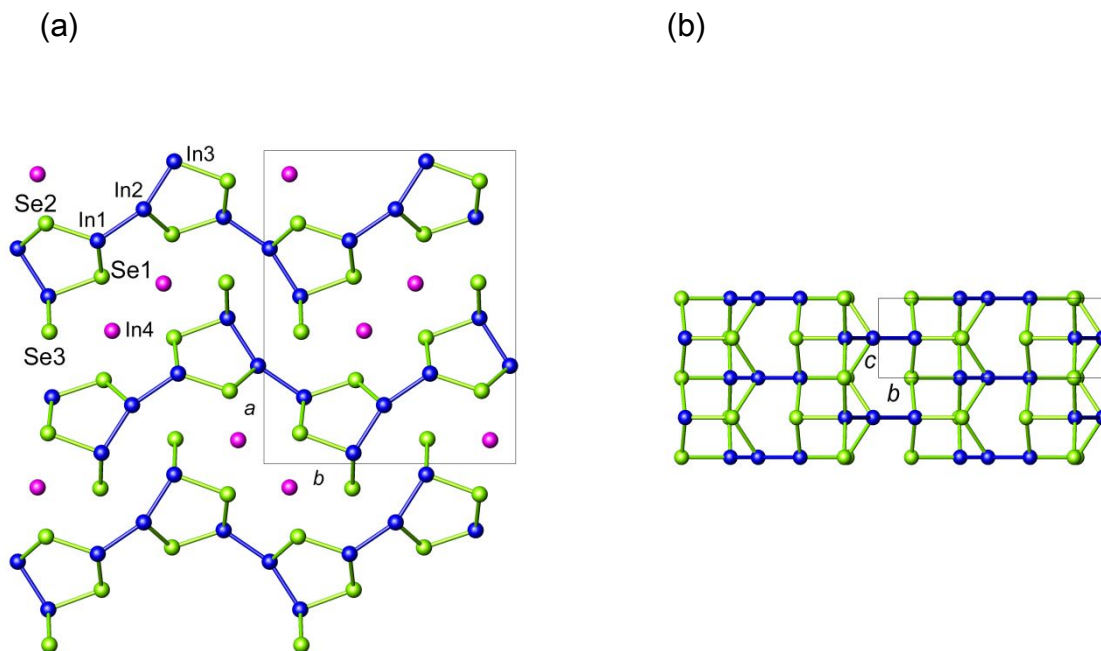


Figure 1. (a) View of the crystal structure of In_4Se_3 along $[001]$. The In1, In2, In3 atoms (dark blue spheres) form $(\text{In}_3)^{5+}$ clusters and are covalently bonded to the selenium atoms (green spheres). The In4 atoms (dark pink spheres) are located between the $[(\text{In}_3)^{5+}(\text{Se}^{2-})_3]^-$ layers. (b) View of a $[(\text{In}_3)^{5+}(\text{Se}^{2-})_3]^-$ layer along $[100]$. The unit cell is shown as a grey rectangle.

The low thermal conductivity of selenium-deficient $\text{In}_4\text{Se}_{3-\delta}$ has been proposed that is the result of charge density wave (CDW) induced by a quasi-one-dimensional lattice Peierls distortion¹⁷. This, however, has been questioned by Osters and co-workers³³, who found that In_4Se_3 behaves as a line phase and does not accommodate selenium deficiency. Instead, selenium-deficient

1
2
3 samples were found to contain indium metal³², while single-crystal X-ray diffraction data provide
4
5
6
7 no evidence of a CDW³³. Moreover, given that stoichiometric In_4Se_3 already exhibits an
8
9
10 unusually low thermal conductivity, the investigation of the origin of the low thermal conductivity
11
12
13
14 of this material is essential.

15
16
17 There is a strong link between the elastic properties and the lattice thermal conductivity of a
18
19
20 given material³⁴, but little is known about the elastic properties of In_4Se_3 ^{35,36}. Here we describe
21
22
23
24 the correlation between structure and elastic and thermal properties of polycrystalline In_4Se_3 .
25
26
27
28 With the aid of first-principles calculations, we explore the interplay between bonding, phonon
29
30
31 dispersions, and mechanical properties in this material. Our results demonstrate that soft
32
33
34
35 bonding of In^+ ions in the pseudo-layered structure of In_4Se_3 is key to interpret the root of low
36
37
38 thermal conductivity in this material.
39
40
41

42 **EXPERIMENTAL**

43 *Synthesis and structural characterization*

44
45
46
47
48
49 The synthetic procedure for the preparation of In_4Se_3 and the Rietveld refinement using
50
51
52 powder X-ray diffraction data were presented in previous work³². Powder X-ray diffraction data
53
54

1
2
3 for the powder and the pellet have been included as Supporting Information (SI, Figure S1).

4
5
6
7 Significant bond lengths and angles are included in the SI (Table S1&2). SEM and EDS

8
9
10 measurements are consistent with the nominal composition of In_4Se_3 (SI, Table S3).

11 12 13 14 *Property measurements*

15
16
17 A pellet (density >95%) with a diameter of 10 mm and a thickness of ~ 2.47 mm was used to

18
19
20 measure the longitudinal and transverse acoustic velocities using an ultrasonic instrument

21
22
23 Panametrics Epoch III. Details of this measurement technique are given elsewhere³⁷. These

24
25
26 measured velocities were used to calculate the elastic parameters, and the Poisson ratio³⁸. The

27
28
29 average sound velocity of the sample was calculated from the longitudinal (v_l) and the

30
31
32 transverse (v_t) sound velocities using the following expression^{39,40}:

$$33
34
35
36
37
38
39
40
41
42
43
44
45
46
47
48
49
50
51
52
53
54
55
56
57
58
59
60
$$v_a = \left(\frac{1}{3} \left[\frac{1}{v_l^3} + \frac{2}{v_t^3} \right] \right)^{-1/3} \quad (1)$$$$

These values were also used to calculate the Poisson ratio (ν_p) using the following

relationship⁴¹:

$$48
49
50
51
52
53
54
55
56
57
58
59
60
$$\nu_p = \frac{1 - 2\left(\frac{v_t}{v_l}\right)^2}{2 - 2\left(\frac{v_t}{v_l}\right)^2} \quad (2)$$$$

The elastic (γ_e) parameter, and Young's modulus (E) were calculated using the equations⁴²:

$$\gamma_e = \frac{3}{2} \left(\frac{1 + v_p}{2 - 3v_p} \right) \quad (3)$$

$$E = \frac{\rho v_s^2 (3v_l^2 - 4v_t^2)}{(v_l^2 - v_t^2)} \quad (4)$$

where ρ is the density of the material. To estimate the Debye temperature, θ_D , the average sound velocity was used in the expression³⁹:

$$\theta_D = \frac{h}{k_B} \left(\frac{3N}{4\pi V} \right)^{-1/3} v_a \quad (5)$$

where V is the unit-cell volume; N is the number of atoms in a unit cell; k_B is the Boltzmann constant, and h is the Plank constant.

The electrical and thermal conductivities were measured and presented in ref³². The electronic (κ_e) and lattice (κ_{lat}) thermal conductivities were estimated using the electrical conductivity data³² in conjunction with the Wiedemann-Franz law:

$$\kappa_e = L\sigma T \quad (6)$$

where σ is the electrical conductivity and L is the Lorenz number. The value of the Lorenz number⁴³ was estimated using the expression $L = 1.5 + \exp[-|S|/116]$, where L is in $10^{-8} \text{ W } \Omega \text{ K}^{-2}$ and S in $\mu\text{V K}^{-1}$

The minimum lattice thermal conductivity $\kappa_{lat, \min}$ of In_4Se_3 was estimated taking into account that⁴⁴:

$$\kappa_{lat} = \frac{1}{3} C_v v_a \Lambda \quad (7)$$

(where C_v and Λ are the volumetric isochoric heat capacity and the phonon mean free path),
by using the interatomic distance as the minimum phonon mean free path. $\kappa_{\text{lat, min}}$ was also
estimated at a high temperature limit using Cahill's model^{14,45}:

$$\kappa_{\text{min}} = \frac{1}{2} \left(\frac{\pi}{6} \right)^{1/3} k_B V^{-2/3} (v_l + 2v_t) \quad (8)$$

First principle calculations

Band structure, density of states, and phonon dispersions were computed using the Quantum
EXPRESSO package⁴⁶ as integrated in AFLOW π ⁴⁷. The Perdew-Burke-Ernzerhof (PBE)
functional was used to describe the exchange-correlation potential. Optimized norm-conserving
PBE pseudopotentials⁴⁸, with a well-converged basis, set corresponding to an energy cut-off of
80 Ry, were used for the wavefunctions. To integrate over the Brillouin zone, a $2 \times 4 \times 8$ (shifted)
grid was used. Electronic transport coefficients were evaluated with PAOFLOW⁴⁹. The finite
difference method using a $1 \times 2 \times 4$ supercell was employed to compute phonons. AFLOW π
uses ElaStic⁵⁰ to determine the nine independent elastic constants, C_{ij} , of orthorhombic crystals
with $Pnmm$ space group. The Young modulus and the Poisson ratio were calculated based on

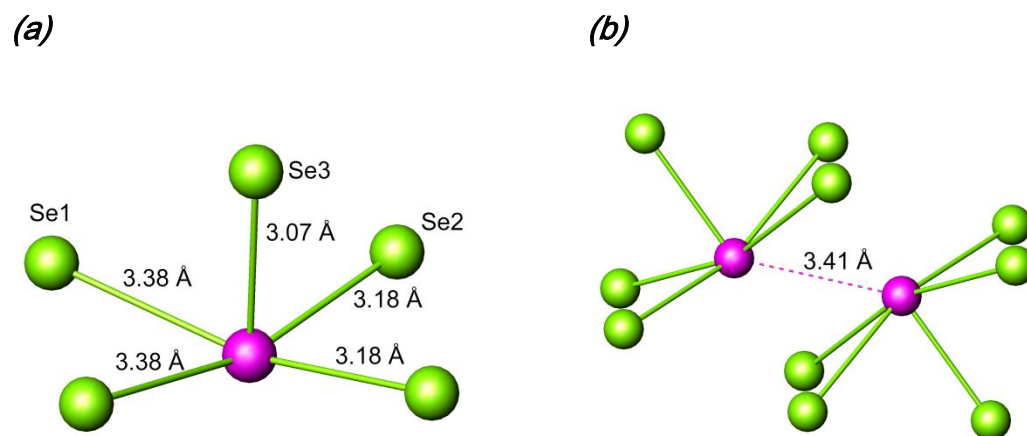
1
2
3 the C_{ij} , by using the Voigt, Reuss, and Hill equations of state. The mode resolved Grüneisen
4
5
6
7 parameters were computed within the quasi-harmonic approximation and the lattice thermal
8
9
10 conductivity was estimated using the Debye-Callaway model⁵¹.

14 RESULTS AND DISCUSSION

17 *Structure and bonding*

21 In_4Se_3 can be formulated as $(\text{In}^+)[(\text{In}_3)^{5+}(\text{Se}^{2-})_3]^-$, indicating the coexistence of covalent and
22
23
24 ionic bonding⁵². The crystal structure of In_4Se_3 (Figure 1) contains anionic layers, perpendicular
25
26
27 to the a-axis, with stoichiometry $[(\text{In}_3)^{5+}(\text{Se}^{2-})_3]^-$. These layers consist of interlocked pentameric
28
29 In_3Se_2 rings, oriented along the c-axis, and linked into bulked layers by linear $(\text{In}_3)^{5+}$ cations.
30
31
32 Within the $(\text{In}_3)^{5+}$ cluster, the distance between In1 and In2 atoms (refer to Figure 1 for atom
33
34 labels) is 2.7239(7) Å while the distance between In2 and In3 is 2.7703(6) Å. These values are
35
36 well below those found in indium metal (3.252 and 3.377 Å)⁵³, and are comparable to the sum
37
38 of the covalent radius for two indium atoms, which is 2.88 Å. Within this layer, the In-Se bond
39
40 distances (SI, Table S1) are also close to the sum of covalent radii for indium (1.44 Å) and
41
42 selenium (1.20 Å)⁵⁴. This indicates that strong covalent bonding occurs within the $[(\text{In}_3)^{5+}(\text{Se}^{2-})_3]^-$
43
44
45
46
47
48
49
50
51
52
53
54

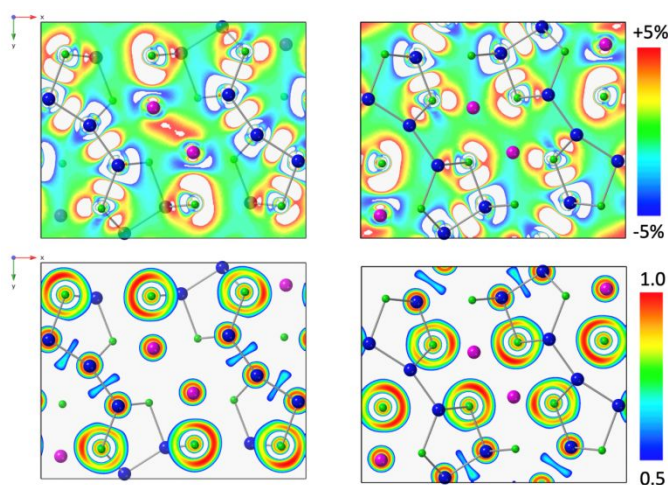
1
2
3
4 layers. Assuming tetrahedral coordination for the selenium atoms, Se3 exhibits two In-Se bonds
5
6
7 and two dangling bonds (unoccupied coordination sites) whilst Se1 and Se2 possess three In-
8
9
10 Se bonds one dangling bond (Figure 1).



16
17
18
19
20
21
22
23
24
25
26
27
28
29
30
31 **Figure 2.** (a) Coordination environment of In4. (b) View of the In4-In4 interaction. Key: In4, dark
32
33
34 pink spheres; selenium, green spheres.

35
36
37
38
39 Bond valence sums are consistent with a lower oxidation state for In4 (SI, Table S2). This
40
41
42 atom, which has a formal oxidation state of In^+ (electronic configuration $[\text{Kr}]5s^2$), is located
43
44
45 between the layers. The distance between In4 and the nearest indium atoms within the layers,
46
47
48 In1 and In2, are 3.8379(7) Å and 3.7530(7), respectively, which are considerably larger than
49
50
51 those in indium metal. The In4-Se distances are also considerably longer than those within the
52
53
54

1
2
3
4 $[(\text{In}_3)^{5+}(\text{Se}^{2-})_3]^-$ layers. In4 adopts distorted square-pyramidal coordination (Figure 2(a)), with In-
5
6
7 Se distances ranging between 3.0688(1) and 3.3802(1) Å (SI, Table S1). These are close to the
8
9
10 sum of ionic radii for In^+ (1.32 Å)⁵⁵, and Se^{2-} (1.98 Å)⁵⁶. This suggests that In^+ cations are held
11
12
13
14 between the layers by electrostatic interactions, while the $[(\text{In}_3)^{5+}(\text{Se}^{2-})_3]^-$ layers are connected
15
16
17 by strong and directional covalent bonds.
18
19
20



21
22
23
24
25
26
27
28
29
30
31
32
33
34
35
36
37
38
39 **Figure 3.** Charge density (top) and ELF (bottom) contour plots in the [001] planes crossing the
40
41 *c*-axis at fractional coordinates of 0.0 (left) and 0.5 (right). The charge density color scale is
42
43 centered on the mean value. Meaningful values of the ELF range from 0.5 to close to 1.0. Ions
44
45
46 are colored as in Figure 1.
47
48
49
50
51
52
53
54
55
56
57
58
59
60

1
2
3
4 The different nature of the bonding of In4 is reflected in its considerably larger atomic
5
6
7 displacement parameter than those for the $(\text{In}_3)^{5+}$ cation found in the covalent layers, evident in
8
9
10 single-crystal diffraction studies³³. For instance, the atomic displacement parameter for In4 found
11
12
13
14 by Osters and coworkers³³ is 60% larger than those in the $(\text{In}_3)^{5+}$ cation.
15
16

17
18 The above considerations are entirely consistent with the results arising from first-principles
19
20
21 electronic structure calculations. The band structure (SI, Figure S3) is in agreement with
22
23
24 previously reported results⁵⁷, with the density of states at the top of the valence band dominated
25
26
27 by Se p and In4 s states. The presence of anti-bonding states with a substantial degree of cation
28
29
30
31 s character at the top of the valence band is a distinctive feature of semiconductors containing
32
33
34 elements with lone pairs⁵⁸, such as the In^+ cation present in In_4Se_3 . The electrical conductivity
35
36
37 and the Seebeck coefficients computed as a function of the chemical potential from 300 to 700
38
39
40
41 K can be found in the SI (Figure S4).
42
43
44

45
46 Figure 3 shows contour plots of the valence charge density and the electron localization factors
47
48
49 (ELF) in two [001] planes. The covalent nature of the bonding within the $[(\text{In}_3)^{5+}(\text{Se}^{2-})_3]^-$ layers is
50
51
52 reflected in the valence charge concentrated in the middle of the In-In and In-Se bonds within
53
54

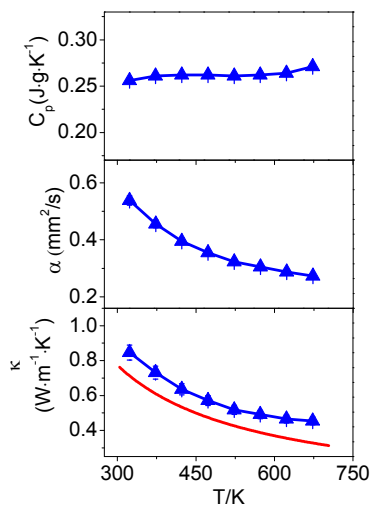
1
2
3 these layers, which is evident in these plots. The dangling bonds associated with the selenium
4
5
6
7 atoms are also clearly observable, as asymmetrically localized electron clouds. By contrast, the
8
9
10 nearly spherical ELF around In4 is consistent with ionic bonding. The square-pyramidal
11
12
13 coordination of In4 would be consistent with the presence of a lone pair of $5s^2$ electrons at the
14
15
16 missing octahedral vertex. Along the direction of this missing vertex, each In4 atom has a
17
18
19
20
21 neighboring In4 at a distance of 3.4082(3) Å (Figure 2(b)). While this distance is larger than
22
23
24 those in the $(\text{In}_3)^{5+}$ cluster, it is of the same order as those found in In metal. In the valence
25
26
27 charge plot (Figure 3), there is evidence of charge concentrated between pairs of In4 atoms,
28
29
30
31 suggesting that these may be forming dimers.
32
33
34
35

36 *Thermal conductivity*

37
38

39 The heat capacity, thermal diffusivity, and total thermal conductivity of polycrystalline In_4Se_3
40
41
42 as a function of temperature (Figure 4), previously presented in³², are in good agreement with
43
44
45 previous reports^{28,29}. The lattice thermal conductivity is the main contributor ($\kappa_{\text{latt}} \sim 99.0\%$) to the
46
47
48 total thermal conductivity of In_4Se_3 (Table 1). The temperature dependence of the thermal
49
50
51 conductivity computed with the Debye-Callaway model (Figure 4) is in superb coincidence with
52
53
54
55

1
2
3 the experimental values. By using the interatomic distance as the phonon mean free path ($\Lambda \sim$
4
5
6
7 3.2 Å), we estimated that $\kappa_{lat,min}$ for In_4Se_3 is $\sim 0.3 \text{ W}\cdot\text{m}^{-1}\cdot\text{K}^{-1}$ at room temperature, while with
8
9
10 Cahill's model, a value of $\kappa_{lat,min}$ of $\sim 0.4 \text{ W}\cdot\text{m}^{-1}\cdot\text{K}^{-1}$ is found. Our experimental value of κ_{lat} is \sim
11
12
13
14 0.84 $\text{W}\cdot\text{m}^{-1}\cdot\text{K}^{-1}$ at 323 K (Table 1), indicating that Λ of In_4Se_3 is larger than the interatomic
15
16
17 distance. Therefore, there is still potential for further reductions in thermal conductivity. Indeed,
18
19
20
21 the incorporation of nano-inclusions in In_4Se_3 ²⁷ leads to values of thermal conductivity close to
22
23
24 its minimum value.
25
26
27



28
29
30
31
32
33
34
35
36
37
38
39
40
41
42
43
44
45 **Figure 4.** The specific heat, thermal diffusivity, and thermal conductivity of In_4Se_3 as a function
46
47
48 of temperature (blue triangles). The temperature dependence of the thermal conductivity
49
50
51
52
53
54
55
56
57
58
59
60

1
2
3
4 computed with the Debye-Callaway model using parameters from the first-principles is shown
5
6
7 as a red line.
8
9

10
11 **Table 1.** The electrical conductivity (σ), electronic thermal (κ_e), lattice thermal (κ_{lat}), and total
12
13
14
15 thermal (κ_{tot}) conductivities at 323 K.
16
17

	σ (S/m)	κ_e ($\text{W}\cdot\text{m}^{-1}\cdot\text{K}^{-1}$)	κ_{lat} ($\text{W}\cdot\text{m}^{-1}\cdot\text{K}^{-1}$)	κ_{tot} ($\text{W}\cdot\text{m}^{-1}\cdot\text{K}^{-1}$)
In_4Se_3	1965	0.01	0.84	0.85

18 19 20 21 22 23 24 25 26 *Elastic properties* 27

28
29
30 The nine elastic constants calculated by us are consistent with the experimental results
31
32
33 reported in the literature (Table 2). The elastic properties for In_4Se_3 determined experimentally
34
35
36 and through our first-principles calculations are summarized in Table 3. The experimentally-
37
38
39 determined sound velocities for In_4Se_3 , which in the Debye model would correspond to the group
40
41
42 velocities of the heat-carrying acoustic phonons, are rather low. These velocities are reasonably
43
44
45 consistent with the calculated values of the transverse sound velocities, 1381 and 1650 m s^{-1} ,
46
47
48 and the longitudinal sound velocity, 2870 m s^{-1} . Given that it has been shown that κ_{lat} is directly
49
50
51
52
53
54
55
56
57
58
59
60

1
2
3
4 proportional to the cube of the average sound velocity⁵⁹, a low sound velocity will result in a low
5
6
7 thermal conductivity. The Young's modulus of In_4Se_3 ($E \sim 47$ GPa), which is related to its
8
9
10 stiffness (i.e. its chemical bond strength), is also low. For instance, the Young's modulus of
11
12
13 In_4Se_3 is significantly lower than those of established thermoelectric materials such as
14
15
16 $\text{Si}_{0.8}\text{Ge}_{0.2}$ ⁶⁰ ($E \sim 143$ GPa) and Mg_2Si ⁶¹ ($E \sim 117$ GPa), and comparable to other state-of-the art
17
18
19 thermoelectric materials, including SnSe ³⁷ ($E \sim 28-40$ GPa), PbSe ³⁷ ($E \sim 62-65$ GPa), PbTe ^{37, 62}
20
21
22 ($E \sim 54-57$ GPa), Cu_2Se ⁶³ ($E \sim 65-68$ GPa) or those of glass and porous materials, such as
23
24
25 borosilicate glass ($E \sim 61-64$ GPa), brick ($E \sim 10-50$ GPa) and concrete ($E \sim 25-38$ GPa)⁶⁴.
26
27
28
29
30
31

32 **Table 2.** Elastic constants for In_4Se_3 in GPa. The experimental data are from ref.³⁶
33
34
35

	C_{11}	C_{22}	C_{33}	C_{44}	C_{55}	C_{66}	C_{12}	C_{13}	C_{23}
This study	37.6	66.7	56.7	13.7	23.7	19.9	17.9	28.0	15.4
Experimental	38.2	66.5	64.3	16.6	26.6	19.0	10.8	30.4	22.4

36
37
38
39
40
41
42
43
44 Materials with weak interatomic bonding usually possess low stiffness and Young's modulus.
45
46
47 They are regarded as "softly" bonded materials that result in flattened phonon dispersion curves,
48
49
50 and therefore, low sound velocities and low thermal conductivities⁶⁵. Theoretically, the value of
51
52
53
54
55
56
57
58
59
60

1
2
3
4 Young's modulus is computed assuming a specific equation of state (EoS), and the calculated
5
6
7 values using the Voigt, Reuss, and Hill EoS are consistent with the experimental results (Table
8
9
10 3). For the three EoS, the calculated Poisson ratios (Table 3) are also in excellent agreement
11
12
13 with the experimental values. The Debye temperature (θ_D) of In_4Se_3 , which is related to the
14
15
16 maximum phonon frequency ($\omega_D = \frac{k_B}{\hbar}\theta_D$), is low, ~ 198 K. This is also consistent with the low
17
18
19 thermal conductivity this material exhibits. The phonon dispersion curves for In_4Se_3 computed
20
21
22 from first principles are presented in Figure 5. The absence of negative branches in the
23
24
25 vibrational spectrum indicates that the structure is thermodynamically stable. Therefore, a
26
27
28 distortion leading to a superstructure is not expected for stoichiometric In_4Se_3 . This is entirely
29
30
31 consistent with the structural study of Osters and coworkers³³, who found no evidence of a
32
33
34 Peierls-distortion or a CDW in stoichiometric In_4Se_3 . It is also noticeable that the frequency of
35
36
37 the acoustic modes is very low, suggesting that the bonding is soft with a substantial number of
38
39
40 low-frequency optical modes, close in energy to the acoustic modes. Although, *per se*, the
41
42
43 vibrational spectrum is not sufficient to determine thermal transport quantities, the small energy
44
45
46 difference between optical and acoustic modes suggests that the low-frequency optical phonon
47
48
49
50
51
52
53
54

1
2
3
4 modes will interact strongly with the heat-carrying acoustic phonons, and may therefore be
5
6
7 interpretative for the low thermal conductivity. By projecting the phonon density of states onto
8
9
10 each atom, we find that the main contributors to low-frequency modes are the indium atoms,
11
12
13 and in particular In4. This is consistent with the weak bonding we found for this atom in our
14
15
16 structural analysis. Visualisations of the atom displacements for selected low-energy optical
17
18
19 modes, together with the vibrational DOS resolved along different directions in the crystal
20
21
22 structure, have been included as SI (Figure S5-S9). These indicate that the In4 atoms move
23
24
25 mainly in the *ab* plane. The large contribution of In4 to the eigendisplacement of the modes at
26
27
28 low frequency is indicative of Einstein-like vibrations reminiscent of rattling. It is widely
29
30
31 recognized that localized rattler modes within the acoustic range reduce the lattice thermal
32
33
34 conductivity, either by resonant scattering or by a reduction in group velocity⁶⁶. Given that our
35
36
37 analysis of the bonding suggests the presence of In4 dimers, these rattling vibrations might
38
39
40
41
42
43
44
45 involve pairs of In4 atoms.
46
47
48
49
50
51
52
53
54
55
56
57
58
59
60

Table 3. Experimentally and computationally determined elastic properties of In_4Se_3 .

Polycrystalline In_4Se_3	Sound velocity (m/s)			Derived parameters		
	v_l	v_t	v_a	Poisson ratio (ν_p)	Young's modulus E (GPa)	θ_D (K)
Experimental	3150	1810	2010	0.25	47	198
Computational	2870	1516 ^a	1695	0.26 ^b	45.58 ^b	
				0.28 ^c	36.56 ^c	
				0.27 ^d	42.59 ^d	

^a Average transverse velocity; ^b Voigt equation of state; ^c Reuss equation of state; ^d Hill equation of state

Anharmonic Effects

First-principles calculations within the quasi-harmonic approximation can be exploited to determine the mode-resolved Grüneisen parameter, which provides a direct measure of the

1
2
3 anharmonicity of bonds (Figure 6(a)). We have demonstrated in the past^{67,68,69} that the presence
4
5
6
7 of low-frequency anharmonic modes is a good descriptor for low thermal conductivity.
8
9
10 Anharmonicity increases phonon-phonon scattering and therefore reduces the lattice thermal
11
12
13 conductivity. As evidenced by Figure 6(a), the mode-resolved Grüneisen parameter for In_4Se_3
14
15
16 is considerably larger for In atoms than for Se atoms. Moreover, the largest values of the
17
18
19 Grüneisen parameter are found for In4 between 20 and 50 cm^{-1} . In the atom-projected vibrational
20
21
22 density of states (Figure 5), this frequency range corresponds to the region where the Einstein-
23
24
25 like dispersion is observed. This is consistent with the weak bonding of In4 resulting in rattling-
26
27
28 like vibrations. Calculations of the total energy response to the in-plane displacement of In4
29
30
31 (Figure 6(b)) indicate that the total energy is minimally affected by displacements, and therefore
32
33
34 confirm that the bonding of this atom is soft. It has been shown that anharmonicity can be
35
36
37 amplified by lone-pair polarization⁷⁰, which could be a contributive factor to the origin of the low
38
39
40 thermal conductivity of In_4Se_3 , owing to the presence of a lone $5s^2$ pair in In4. Our structural
41
42
43 analysis suggests that the In4 atoms, which exhibit a highly asymmetric bonding environment,
44
45
46 might be forming weakly-interacting dimers (Figure 2). We conjecture that, during thermal
47
48
49
50
51
52
53
54

vibrations, the interaction of the lone pairs along the In4...In4 direction will lead to high anharmonicity.

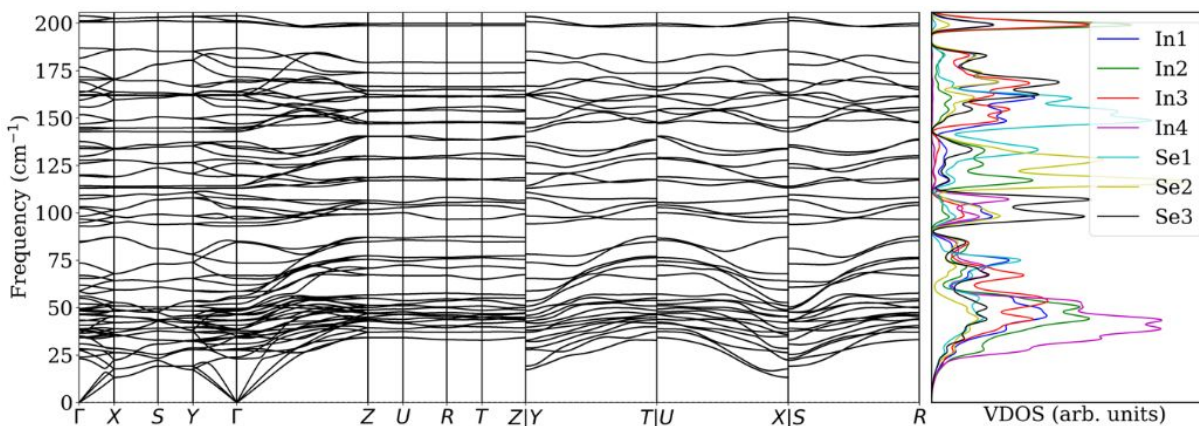


Figure 5. The computed phonons dispersion curves (left) for In_4Se_3 from first-principles and atom-projected vibrational density of states (right). LO-TO splitting is very small.

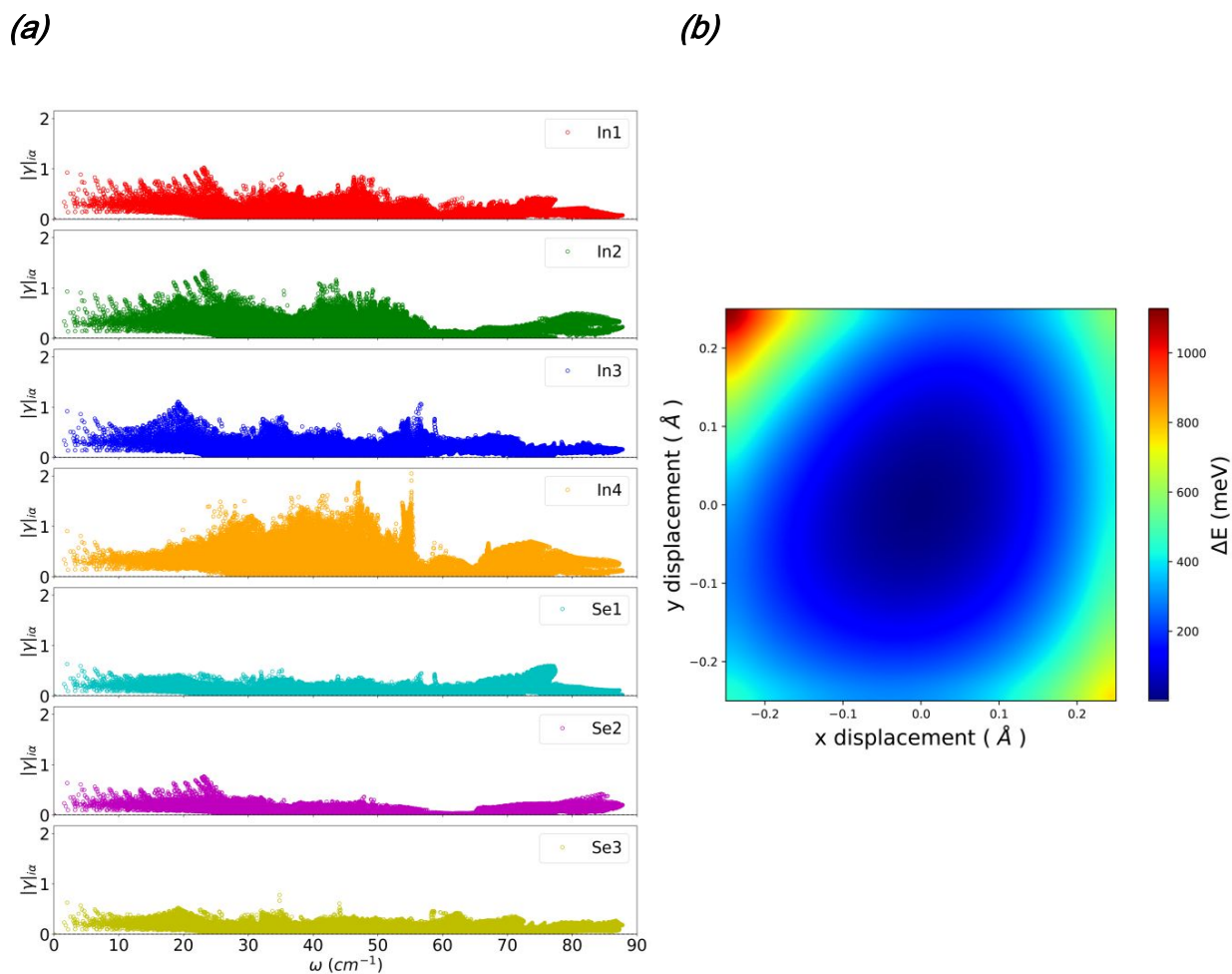


Figure 6. (a) Mode resolved Grüneisen parameters projected on individual atoms. (b) Total energy differences for the symmetrized displacement of the In4 atom along the [001] direction and in the plane x-y.

CONCLUSIONS

Our experimental and computational results demonstrate that, contrary to a previous suggestion which related low thermal conductivity to a Peierls distortion¹⁷, the intrinsically low thermal conductivity of In_4Se_3 is a consequence of the soft bonding of In^+ ions located between covalently-bonded $[(\text{In}_3)^{5+}(\text{Se}^{2-})_3]^-$ layers. This conclusion is strongly supported by the presence of Einstein-like modes in the vibrational density of states, which we attribute to “rattling” vibrations of the weakly-bonded In^+ cations. The synergistic effect of soft bonding and the lone $5s^2$ pair of the In^+ cations leads to a high degree of anharmonicity, as evidenced by large mode-resolved Grüneisen parameters, and hence to more effective phonon scattering.

ACKNOWLEDGMENTS

S. D. N. L and K.T.W thank the Institute of Advanced Manufacturing Technology for hosting and financial support within the TEAM –TECH0076 project of the Foundation for Polish Science, entitled “New approach for the development of efficient materials for direct conversion of heat into electricity project”, co-financed by the European Union under the European Regional Development Fund. P.V. acknowledges The Leverhulme Trust for Research Project Grant

1
2
3 (RPG-2019-288). A.R.S. and M.F. thank the Institute for Cyber-Enabled Research at Michigan
4
5
6
7 State University for access to computational facilities, and Giovanni Pizzi at materialscloud.org
8
9
10 for technical support.

11 12 13 14 **Supporting Information**

15
16
17
18
19 The following files are available free of charge:

20
21
22
23
24 Tables of bond lengths and angles, bond valence sums, powder XRD of powdered and pellet
25
26
27 samples, SEM and EDS data, the calculated electronic structure, calculated Seebeck and
28
29
30 electrical conductivity, the visualisations of the atom displacements, and vibrational DOS data
31
32
33
34 (PDF).
35
36
37

38 **AUTHOR INFORMATION**

39 40 **Corresponding Author**

41
42
43
44
45 *E-mail: luudngocson@duytan.edu.vn; p.vaqueiro@reading.ac.uk
46
47
48

49 **Author Contribution**

50
51
52 The manuscript was written through the contributions of all authors.
53
54

1
2
3 **Notes**
4
5

6 The authors declare that they have no known competing financial interests or personal
7 relationships that could have appeared to influence the work reported in this paper.
8
9
10
11
12
13
14
15
16
17
18
19
20
21
22
23
24
25
26
27
28
29
30
31
32
33
34
35
36
37
38
39
40
41
42
43
44
45
46
47
48
49
50
51
52
53
54

REFERENCES

- (1) Rowe, D. M., *Thermoelectrics Handbook: Macro to Nano*, ed. D. M. Rowe, CRC Press, Taylor and Francis, Boca Raton, 2006, 1.
- (2) Slack, G. A., New materials and performance limits for thermoelectric cooling. In *CRC Handbook of Thermoelectrics*; Rowe, D.M., Ed.; CRC, Boca Raton, 1995, **34**, 407-440.
- (3) Yin, Y., Baskaran, K., Tiwari, A., A Review of Strategies for Developing Promising Thermoelectric Materials by Controlling Thermal Conduction, *Phys. Status Solidi A*, 2019, 1800904
- (4) Yang, J., Wang, Y., Yang, H., Tang, W., Yang, J., Chen, L., Zhang, W., Thermal transport in thermoelectric materials with chemical bond hierarchy, *J. Phys.: Condens. Matter*, 2019, **31**, 183002
- (5) Liu, H., Shi, X., Xu, F., Zhang, L., Zhang, W., Chen, L., Li, Q., Uher, C., Day, T., Snyder, G.J., Copper ion liquid-like thermoelectrics, *Nat. Mater.*, 2012, **11**, 422-425.

- 1
2
3
4
5 (6) Qiu, W., Xi, L., Wei, P., Ke, X., Yang, J., Zhang, W., Part-crystalline part-liquid state and
6 rattling-like thermal damping in materials with chemical-bond hierarchy, *Proc. Natl. Acad. Sci.*
7
8
9
10
11
12 USA 2014, 111, 15031
13
14
15 (7) Li, D., Zhao, H., Li, Sh., Wei, B., Shuai, J., Shi, Ch., Xi, X., Sun, P., Meng, Sh., Gu, L., Ren,
16
17
18
19 Zh., Chen, X., Atomic Disorders Induced by Silver and Magnesium Ion Migrations Favor High
20
21
22
23 Thermoelectric Performance in α -MgAgSb Based Materials, *Adv. Funct. Mater.* 2015, 25, 6478–
24
25
26 6488
27
28
29 (8) Zhao, K., Qiu, P., Shi, X., Chen, L., Recent Advances in Liquid-Like Thermoelectric Materials,
30
31
32
33 *Adv. Funct. Mater.* 2019, 1903867
34
35
36 (9) Kim, S.I., Lee, K.H., Mun, H.A., Kim, H.S., Hwang, S.W., Roh, J.W., Yang, D.J., Shin,
37
38
39
40 W.H., Li, X.S., Lee, Y.H., Snyder, G.J., Kim, S., Dense dislocation arrays embedded in grain
41
42
43
44 boundaries for high-performance bulk thermoelectrics, *Science*, 2015, **348**, 109-114.
45
46
47 (10) Kim, W., Strategies for engineering phonon transport in thermoelectrics, *J. Mater. Chem.*
48
49
50
51 *C*, 2015, **3**, 10336-10348
52
53
54

1
2
3
4
5 (11) Kanatzidis, M. G., Nanostructured thermoelectrics: The New Paradigm? *Chem. Mater.*,
6
7
8
9 2010, **22**, 648-659.

10
11
12 (12) Samanta, M., Pal, K., Pal, P., Waghmare, U. V., Biswas, K., Localized Vibrations of Bi
13
14
15
16
17 Bilayer Leading to Ultralow Lattice Thermal Conductivity and High Thermoelectric Performance
18
19
20 in Weak Topological Insulator n-Type BiSe, *J. Am. Chem. Soc.* 2018, **140**, 17, 5866–5872.

21
22
23 (13) Acharyya, P., Ghosh, T., Pal, K., Kundu, K., Rana, K. S., Pandey, J., Soni, A., Waghmare,
24
25
26
27
28 U. V., Biswas, K., Intrinsically Ultralow Thermal Conductivity in Ruddlesden–Popper 2D
29
30
31 Perovskite $\text{Cs}_2\text{PbI}_2\text{Cl}_2$: Localized Anharmonic Vibrations and Dynamic Octahedral Distortions,
32
33
34
35 *J. Am. Chem. Soc.* 2020, **142**, 36, 15595–15603.

36
37
38 (14) Sarkar, D., Ghosh, T., Roychowdhury, S., Arora, R., Sajan, S., Sheet, G., Waghmare, U.
39
40
41
42
43 V., Biswas, K., Ferroelectric Instability Induced Ultralow Thermal Conductivity and High
44
45
46 Thermoelectric Performance in Rhombohedral p-Type GeSe Crystal, *J. Am. Chem. Soc.* 2020,
47
48
49 **142**, 28, 12237–12244.

1
2
3
4
5 (15) Dutta, M., Matteppanavar, S., Prasad, M. V. D., Pandey, J., Warankar, A., Mandal, P.,
6
7
8
9 Soni, A., Waghmare, U. V., Biswas, K., Ultralow Thermal Conductivity in Chain-like TlSe Due to
10
11
12 Inherent Tl⁺ Rattling, *J. Am. Chem. Soc.* 2019, **141**, 51, 20293–20299.
13

14
15
16 (16) Rathore, E., Juneja, R., Culver, S. P., Minafra, N., Singh, A. K., Zeier, W. G., Biswas, K.,
17
18
19
20 Origin of Ultralow Thermal Conductivity in n-Type Cubic Bulk AgBiS₂: Soft Ag Vibrations and
21
22
23 Local Structural Distortion Induced by the Bi 6s² Lone Pair, *Chem. Mater.* 2019, **31**, 6, 2106–
24
25
26
27 2113.
28

29
30
31 (17) Rhyee, J. S., Lee, K.H., Lee, S. M., Cho, E., Kim, S. I., Lee, E., Kwon, Y. S., Shim, J. H.,
32
33
34
35 Kotliar, G., Peierls distortion as a route to high thermoelectric performance in In₄Se_{3-δ} crystals,
36
37
38 *Nature*, 2009, **459**, 965.
39

40
41
42 (18) Rhyee, J. S., Ahn, K., K.H., Lee, Ji, H. S., Shim, J.H., Enhancement of the Thermoelectric
43
44
45
46 Figure-of-Merit in a Wide Temperature Range in In₄Se_{3-x}Cl_{0.03} Bulk Crystals, *Adv. Mater.*, 2011,
47
48
49 **23**, 2191.
50

1
2
3
4
5 (19) Lin, Z. S., Chen, L., Wang, L. M., Zhao, J. T., Wu, L. M., A Promising Mid-Temperature
6
7
8
9 Thermoelectric Material Candidate: Pb/Sn-Codoped $\text{In}_4\text{Pb}_x\text{Sn}_y\text{Se}_3$ *Adv. Mater.*, 2013, **25**, 4800
10
11
12 – 4806.
13

14
15
16 (20) Han, G., Chen, Z-G., Drennan, J., Zou, J., Indium Selenides: Structural Characteristics,
17
18
19
20 Synthesis and Their Thermoelectric Performances, *Small*, 2014, **14**, 10, 2747-2765.
21
22

23
24 (21) Yin, X., Liu, J-Y., Chen, L., Wu, L-M., High Thermoelectric Performance of In_4Se_3 -Based
25
26
27
28 Materials and the Influencing Factors, *Acc. Chem. Res.*, 2018, **51**, 2, 240-247.
29
30

31
32 (22) Ahn, K., Cho, E., Rhyee, J. S., Kim, S. Il., Lee, S. M., Lee, K. H., Effect of cationic
33
34
35
36 substitution on the thermoelectric properties of $\text{In}_{4-x}\text{M}_x\text{Se}_{2.95}$ compounds (M=Na, Ca, Zn, Ga,
37
38
39 Sn, Pb; x=0.1), *Appl. Phys. Lett.*, 2011, **99**, 102110.
40
41

42
43 (23) Li, G., Yang, J. Y., Luo, Y. B., Xiao, Y., Fu, L. W., Liu, M., Peng, J. Y., Improvement of
44
45
46
47 Thermoelectric Properties of In_4Se_3 Bulk Materials with Cu Nano-inclusions, *J. Am. Ceram. Soc.*,
48
49
50 2013, **96**, 2703.
51
52

- 1
2
3
4
5 (24) J. Y., Luo, Yang, J. Y., Li, G., Liu, M., Xiao, Y., Fu, L. W., Li, W. X., Zhu, P. W., Peng, J.
6
7
8 Y, Gao, S., Zhang, J. Q., Enhancement of the Thermoelectric Performance of Polycrystalline
9
10 In₄Se_{2.5} by Copper Intercalation and Bromine Substitution, *Adv. Energy Mater.* 2014, **4**,
11
12
13
14
15 1300599.
16
17
18
19
20 (25) Lee, M. H., Rhyee, J. S., Vaseem, M., Hahn, Y. B., Park, S. D., Kim, H. J., Kim, S. J., Lee,
21
22
23 H. J., Kim, C., Thermoelectric properties of SrTiO₃ nano-particles dispersed indium selenide bulk
24
25
26 composites, *Appl. Phys. Lett.*, 2013, **102**, 223901.
27
28
29
30
31 (26) Zhai, Y. B., Zhang, Q. S., Jiang, J., Zhang, T., Xiao, Y. K., Yang, S. H., Xu, G. J.,
32
33
34 Thermoelectric performance of the ordered In₄Se₃-In composite constructed by monotectic
35
36
37 solidification, *J. Mater. Chem. A*, 2013, **1**, 8844-8847.
38
39
40
41
42 (27) Rawat, P. K., Park, H., Hwang, J., Kim, W., Low Thermal Conductivity and High
43
44
45 Thermoelectric Performance in In₄Se_{3-x} with Phase-Separated Indium Inclusions, *J. Elec. Mater.*
46
47
48 2017, **46**, 1444-1450.
49
50
51
52
53
54

1
2
3
4
5 (28) Zhu, G.H., Lan, Y.C., Wang, H., Joshi, G., Hao, Q., Chen, G., Ren, Z.F. , Effect of selenium
6 deficiency on the thermoelectric properties of n-type $\text{In}_4\text{Se}_{3-x}$ compounds, *Phys. Rev. B*, 2011,
7
8
9
10
11
12 **83**, 115201.

13
14
15
16 (29) Ahn, K., Cho, E., Rhyee, J. S., Kim, S. II., Hwang, S., Kim, H-S., Lee, S. M., Lee, K. H.,
17
18
19
20 Improvement in the thermoelectric performance of the crystals of halogen-substituted
21
22
23 $\text{In}_4\text{Se}_{3-x}\text{H}_{0.03}$ (H = F, Cl, Br, I): Effect of halogen-substitution on the thermoelectric properties in
24
25
26
27 $\text{In}_4\text{Se}_{3-x}$ *J. Mater. Chem.*, 2012, **22**, 5730-5736.

28
29
30
31 (30) Kim, J. H., Kim, M. J., Oh, S., Rhyee, J-S., Thermoelectric properties of Se-deficient and
32
33
34
35 Pb-/Sn-codoped $\text{In}_4\text{Pb}_{0.01}\text{Sn}_{0.03}\text{Se}_{3-x}$ polycrystalline compounds, *J. Alloy. Compd.*, 2014, **615**,
36
37
38
39 933–936.

40
41
42 (31) Abharia, A. S., Abdellahib, M., Bahmanpour, M., The effects of Sn-substitution on
43
44
45
46 thermoelectric properties of $\text{In}_{4-x}\text{Sn}_x\text{Se}_3$ ceramic, *Ceram. Int.*, 2016, **42**, 5593–5599.
47
48
49
50
51
52
53
54

1
2
3
4
5 (32) Luu, S. D. N., Parashchuk, T., Kosonowski, A., Phan, T. B., Wojciechowski, K. T.,
6
7
8
9 Structural and Thermoelectric Properties of Solid–Liquid $\text{In}_4\text{Se}_3\text{-In}$ Composite, *J. Elec. Mater.*
10
11
12 2019, **48**, 5418–5427.

13
14
15
16 (33) Osters, O., Blazek, G., Nilges, T., Comments on Peierls-distorted Indium Chains in $\text{In}_4\text{Se}_{3-x}$,
17
18
19
20 *Z. Anorg. Allg. Chem.* 2013, **639**, 497–501.

21
22
23
24 (34) Jia, T., Chen, G., Zhang, Y., Lattice thermal conductivity evaluated using elastic
25
26
27
28 properties, *Phys. Rev. B*, 2017, 95, 155206.

29
30
31
32 (35) Ji, H. S., Kim, H., Lee, C., Rhyee, J-S., Kim, M. H., Kaviany, M., Shim, J. H., Vacancy-
33
34
35
36 suppressed lattice conductivity of high-ZT $\text{In}_4\text{Se}_{3-x}$, *Phys. Rev. B*, 2013, **87**, 125111.

37
38
39
40 (36) Kuryachii, V. Y., Bogachev, V. Y., Mikhal'chenko, V. P., Stakhira, I. M., Elastic properties
41
42
43
44 of In_4Se_3 , *Izv. Akad. Nauk SSSR, Neorg. Mater.* 1986, **18**, 756-757.

45
46
47
48 (37). Zevalkink, A.; Smiadak, D. M.; Blackburn, J. L.; Ferguson, A. J.; Chabinyk, M. L.; Delaire,
49
50
51
52 O.; Wang, J.; Kovnir, K.; Martin, J.; Schelhas, L. T.; Sparks, T. D.; Kang, S. D.; Dylla, M. T.;

1
2
3
4
5 Snyder, G. J.; Ortiz, B. R.; Toberer, E. S. A practical field guide to thermoelectrics:
6
7

8
9 Fundamentals, synthesis, and
10

11
12 characterization, *App. Phys. Rev.* 2018, **5**, 021303.
13

14
15 (38) Asmani, M., Kermel, C., Leriche, A., Ourak, M., Influence of porosity on Young's modulus
16
17 and Poisson's ratio in alumina ceramics, *J. Eur. Ceram. Soc.*, 2001, **21**, 1081-1086.
18
19

20
21 (39) Anderson, O. L., A simplified method for calculating the Debye temperature from elastic
22
23 constants, *J. Phys. Chem. Solids*, 1963, **24**, 909-917.
24
25
26

27
28 (40) Kurosaki, K., Kosuga, A., Muta, H., Uno, M., Yamanaka, S., Ag₉TlTe₅: A high-performance
29
30 thermoelectric bulk material with extremely low thermal conductivity, *Appl. Phys. Lett.*, 2005, **87**,
31
32 061919.
33
34
35
36
37
38

39
40 (41) Sanditov, D. S., Belomestnykh, V. N., Relation between the parameters of the elasticity
41
42 theory and averaged bulk modulus of solids, *Tech. Phys.* 2011, **56**, 1619-1623.
43
44
45
46
47
48
49
50
51
52
53
54

1
2
3
4
5 (42) Belomestnykh, V.N., Tesleva, E.P., Interrelation between anharmonicity and lateral strain
6
7
8 in quasi-isotropic polycrystalline solids, *Tech. Phys.* 2004, **49**, 1098-1100.
9

10
11
12
13 (43) Kim, H.-S.; Gibbs, Z. M.; Tang, Y.; Wang, H.; Snyder, G. J. *APL Materials*, 2015, **3**,
14
15
16 041506.
17

18
19
20
21 (44) Slack, G., Nonmetallic crystals with high thermal conductivity, *J. Phys. Chem. Solids*,
22
23
24 1973, **34**, 321-335.
25

26
27
28 (45) Cahill, D. G., Watson, S. K., Pohl, R. O., Lower limit to the thermal conductivity of
29
30
31 disordered crystals, *Phys. Rev. B* 1992, **46**, 6131-6140
32

33
34
35
36 (46) Giannozzi, P., Baroni, S., Bonini, N., Calandra, M., Car, R., Cavazzoni, C., Ceresoli, D.,
37
38
39 Chiarotti, G. L, Cococcioni, M., Dabo, I., Corso, A. Dal., Gironcoli, S. de, Fabris, S., Fratesi, G.,
40
41
42 Gebauer, R., Gerstmann, U., Gougoussis, C., Kokalj, A., Lazzeri, M., Martin-Samos, L., Marzari,
43
44
45 N., Mauri, F., Mazzarello, R., Paolini, S., Pasquarello, A., Paulatto, L., Sbraccia, C., Scandolo,
46
47
48 S., Sclauzero, G., Seitsonen, A. P., Smogunov, A., Umari, P., Wentzcovitch, R. M., QUANTUM
49
50
51
52
53
54

1
2
3
4
5 ESPRESSO: a modular and open-source software project for quantum simulations of materials,
6
7

8
9 *J. Phys.: Condens. Matter*, 2009, **21**, 395502
10

11
12
13 (47) Supka, A. R., Lyons, T. E., Liyanage, L., D'Amico, P., Al Rahal Al Orabi, R., Mahatara, S.,
14

15
16 Gopal, P., Toher, C., Ceresoli, D., Calzolari, A., Curtarolo, S., Nardelli, M. B., Fornari, M.,
17

18
19 AFLOW π : A minimalist approach to high-throughput ab initio calculations including the
20

21
22 generation of tight-binding hamiltonians, *Comput. Mater. Sci.*, 2017, **136**, 76-84.
23
24

25
26
27 (48) Setten, M. J. V., Giantomassi, M., Bousquet, E., Verstraete, M. J., Hamann, D. R., Gonze,
28

29
30 X., Rignanese, G.-M., The PseudoDojo: Training and grading a 85 element optimized norm-
31

32
33 conserving pseudopotential table, *Comput. Phys. Commun*, 2018, **226**, 39-54.
34
35
36

37
38 (49) Nardelli, M. B., Cerasoli, F. T., Costa, M., Curtarolo, S., De Gennaro, R., Fornari, M.,
39

40
41 Liyanage, L., Supka, A. R., Wang, H., PAOFLOW: A utility to construct and operate on ab initio
42

43
44 Hamiltonians from the projections of electronic wavefunctions on atomic orbital bases, including
45

46
47 characterization of topological materials, *Comp. Mat. Sci.* 2018, **143**, 462-472
48
49
50

- 1
2
3
4
5 (50) Golesorkhtabar, R., Pavone, P., Spitaler, J., Puschnig, P., Draxl, C., ElaStic: A tool for
6
7
8 calculating second-order elastic constants from first principles, *Comput. Phys. Commun.*, 2013,
9
10
11
12 **184**, 1861–1873
13
14
15
16 (51) Zhang, Y., First-principles Debye–Callaway approach to lattice thermal conductivity, *J.*
17
18
19 *Materiomics*, 2016, **2**, 237-247
20
21
22
23
24 (52) Hogg, J. H. C., Sutherland, H. H., Williams, D. J., The crystal structure of tetraindium
25
26
27 triselenide, *Acta Crystallogr. B*, 1973, **B29**, 1590-1593
28
29
30
31
32 (53) Wolcyrz, M., Kubiak, R., Maciejewski, S., X-ray investigation of thermal expansion and
33
34
35 atomic thermal vibrations of tin, indium, and their alloys, *Phys. Status Solidi B*, 1981, **107**, 245-
36
37
38
39 253
40
41
42
43 (54) Cordero, B., Gómez, V., Platero-Prats, A. E., Revés, M., J. Echeverría, E. Cremades,
44
45
46 F.Barragán, S. Alvarez, Covalent radii revisited, *Dalton Trans.*, 2008, **21**, 2832–2838
47
48
49
50
51
52
53
54

- 1
2
3
4
5 (55) Jones, R. E., Templeton, D. H., The crystal structure of indium (I) iodide, *Acta Crystallogr.*
6
7
8
9 1955, **8**, 847
10
11
12
13 (56) Shannon, R. D., Revised effective ionic radii and systematic studies of interatomic
14
15
16 distances in halides and chalcogenides, *Acta Crystallogr A*. 1976, **A32**: 751–767
17
18
19
20
21 (57) Losovyj, Y. B., Makinistian, L., Albanesi, E. A., Petukhov, A. G., Liu, J., Galiy, P., Dveriy,
22
23
24 O. R., Dowben, P. A., The anisotropic band structure of layered In₄Se₃(001), *J. Appl. Phys.*,
25
26
27 2008, **104**, 083713.
28
29
30
31
32 (58) Walsh, A., Payne, D. J., Egdell, R. G., Watson, G. W., Stereochemistry of post-transition
33
34
35 metal oxides: revision of the classical lone pair model, *Chem. Soc. Rev.*, 2011, **40**, 4455–4463
36
37
38
39
40 (59) Hanus, R., Agne, M. T., Rettie, A. J. E., Chen, Z., Tan, G., Chung, D. Y., Kanatzidis, M.G.,
41
42
43 Pei, Y., Voorhees, P. W., Snyder, G. J., Lattice Softening Significantly Reduces Thermal
44
45
46 Conductivity and Leads to High Thermoelectric Efficiency, *Adv. Mater.* 2019, **31**, 1900108
47
48
49
50
51
52
53
54

1
2
3
4
5 (60) Kallel, A.C., Roux, G., Martin, C.L., Thermoelectric and mechanical properties of a hot
6 pressed nanostructured n-type Si₈₀Ge₂₀ alloy, *Mater. Sci. Eng. A.*, 2013, **564**, 65-70
7
8

9
10
11
12
13 (61) Schmidt, R., Fan, X., Case, E., Sarac, P., Mechanical properties of Mg₂Si thermoelectric
14 materials with the addition of 0–4 vol% silicon carbide nanoparticles (SiCNP), *J. Mater. Sci.*,
15
16
17
18
19
20 2015, **50**, 11, 4034-4046
21
22
23

24 (62) Ni, E. J., Casea, D.E., Khabir, N.K., Stewart, C.R., Wub, Ch-I., Hoganb, P.T., Timmc, J.
25
26
27
28 E., Giraridd, N.S., Kanatzidis, G. M., Room temperature Young's modulus, shear modulus,
29
30
31
32 Poisson's ratio and hardness of PbTe–PbS thermoelectric materials, *Mat. Sci. Eng. B*, 2010,
33
34
35 170, 58–66
36
37

38 (63) Li, M. Kazi Nazrul Islam, Md. Sh., Yahyaoglu, M., Pan, D., Shi, X., Chen, L.D., Aydemir. U.,
39
40
41
42 Wang, X., Ultrahigh figure-of-merit of Cu₂Se incorporated with carbon coated boron
43
44
45 nanoparticles, *InfoMat*. 2019;1:108–115
46
47
48
49
50
51
52
53
54
55

1
2
3
4
5 (64) Ashby, M. F., *Materials Selection in Mechanical Design*, 4th Edi. Butterworth Heinemann,
6
7
8
9 2011

10
11
12
13 (65) Lin, S., Li, W., Li, S., Zhang, X., Chen, Z., Xu, Y., Chen, Y., Pei, Y., High Thermoelectric
14
15
16 Performance of Ag₉GaSe₆ Enabled by Low Cut off Frequency of Acoustic Phonons, *Joule*, 2017,
17
18
19
20 1, 816-830

21
22
23
24 (66) Toberer, E.S., Zevalkink, A., Snyder, G.J., Phonon engineering through crystal chemistry, *J. Mater.*
25
26 *Chem.*, 2011, **21**, 15843-15852

27
28
29
30 (67) Vaqueiro, P., Al Orabi, R. A. R., Luu, S. D. N., Guélou, G., Powell, A. V., Smith, R. I.,
31
32
33 Song, J.-P., Wee, D., Fornari, M., The Role of Copper in The Thermal Conductivity of
34
35
36 Thermoelectric Oxychalcogenides: Do Lone Pairs Matter?, *Phys. Chem. Chem. Phys.* 2015, **17**,
37
38
39
40 31735- 31740.

41
42
43
44 (68) Plata, J. J., Nath, P., Usanmaz, D., Carrete, J., Toher, C., Jong, M. D., Asta, M. D., Fornari,
45
46
47
48 M., Nardelli, M. B., Curtarolo, S., An efficient and accurate framework for calculating lattice
49
50

1
2
3
4
5 thermal conductivity of solids: AAPL - AFLOW Anharmonic Automatic Phonon Library, *NPJ*

6
7
8
9 *Comp. Mat.* 2017, **3**, 45 .

10
11
12
13 (69) Bourgs, C., Bouyrie, Y., Supka, A., Al Orabi, R. A. R, Lemoine, P., Lebedev, O., Ohta, M.,

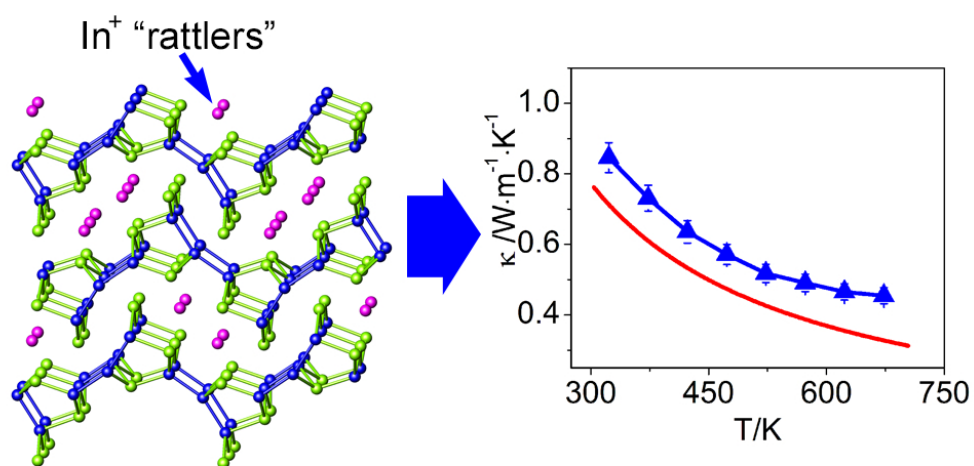
14
15
16 Suekuni, K., Nassif, V., Hardy, V., Daou, R., Miyazaki, Y., Fornari, M., Guilmeau, E., High-

17
18
19 performance Thermoelectric Bulk Colusite by Process Controlled Structural Disordering, *J. Am.*

20
21
22
23 *Chem. Soc.* 2018, **140**, 2186-2195 .

24
25
26
27 (70) Nielsen, M. D., Ozolins, V., Heremans, J. P., Lone pair electrons minimise lattice thermal

28
29
30
31 conductivity, *Energy Environ. Sci.* 2013, **6**, 570-578.



82x44mm (300 x 300 DPI)